

Topological semimetallic phase in PbO_2 promoted by temperatureBo Peng,^{1,2} Ivona Bravić,¹ Judith L. MacManus-Driscoll,³ and Bartomeu Monserrat^{1,*}¹*Cavendish Laboratory, University of Cambridge, J. J. Thomson Avenue, Cambridge CB3 0HE, United Kingdom*²*Key Laboratory of Micro and Nano Photonic Structures (MOE), Department of Optical Science and Engineering, Fudan University, Shanghai 200433, China*³*Department of Materials Science and Metallurgy, University of Cambridge, 27 Charles Babbage Road, Cambridge CB3 0FS, United Kingdom*

(Received 26 July 2019; published 1 October 2019)

Materials exhibiting topological order host exotic phenomena that could form the basis for novel developments in areas ranging from low-power electronics to quantum computers. The past decade has witnessed multiple experimental realizations and thousands of predictions of topological materials. However, it has been determined that increasing temperature destroys topological order, restricting many topological materials to very low temperatures and thus hampering practical applications. Here, we propose a material realization of temperature-promoted topological order. We show that a semiconducting oxide that has been widely used in lead-acid batteries, $\beta\text{-PbO}_2$, hosts a topological semimetallic phase driven by both thermal expansion and electron-phonon coupling upon increasing temperature. We identify the interplay between the quasi-two-dimensional nature of the charge distribution of the valence band with the three-dimensional nature of the charge distribution of the conduction band as the microscopic mechanism driving this unconventional temperature dependence. Thus, we propose a general principle to search for and design topological materials whose topological order is stabilized by increasing temperature. This provides a clear roadmap for taking topological materials from the laboratory to technological devices.

DOI: [10.1103/PhysRevB.100.161101](https://doi.org/10.1103/PhysRevB.100.161101)

Materials exhibiting topological order have the potential to revolutionize modern technology. For example, Chern insulators exhibit the quantum anomalous Hall effect supporting dissipationless currents that could form the basis for low-power electronics [1,2], and topological superconductors sustain Majorana fermions that could provide a platform for robust topological quantum computers [3–6]. The past decade has witnessed the establishment of a solid theoretical foundation of topological order, and the prediction and observation of topological phenomena in a range of materials [7,8].

However, topological phenomena are currently mostly restricted to very low temperatures, precluding most applications. Current experiments invariably show that increasing temperature suppresses topological order [9–13] and this can be rationalized with a combination of thermal expansion and electron-phonon coupling. Although electron-phonon coupling can both promote or suppress topological order [14–21], thermal expansion pushes materials towards the atomic limit which always exhibits a trivial band ordering, and as a result there are no examples of materials in which temperature promotes topological order. This prompts the question, is it possible to identify materials in which temperature promotes rather than suppresses topological order?

We present an example of a temperature-promoted topological phase in $\beta\text{-PbO}_2$. With increasing temperature, *both* thermal expansion and electron-phonon coupling contribute

towards stabilizing a topologically ordered phase in an otherwise trivial semiconductor. Contrary to known topological materials so far, we show that the coexistence of the quasi-two-dimensional real-space charge distribution associated with the valence band of $\beta\text{-PbO}_2$, together with the three-dimensional charge distribution of the conduction band, can promote a topological phase even under thermal expansion. Furthermore, the underlying microscopic mechanism we present in this Rapid Communication can be employed as a guiding principle to identify other materials in which the topological order is robust at high temperatures, thus opening the door for practical room-temperature applications of topological matter.

Our study is based on first-principles density functional theory (DFT) calculations performed using the Vienna *ab initio* simulation package (VASP) [23]. The projector augmented-wave potential is used with Pb $5d^{10}6s^26p^2$ and O $2s^22p^4$ valence states. Hybrid functional methods based on the Heyd-Scuseria-Ernzerhof (HSE06) approximation are adopted [24–26] with 25% of the exact screened Hartree-Fock exchange incorporated into the semilocal exchange within the generalized gradient approximation (GGA) in the Perdew-Burke-Ernzerhof (PBE) parametrization [27]. Based on convergence tests, we use a kinetic energy cutoff set to 500 eV and a Γ -centered $4 \times 4 \times 6$ \mathbf{k} mesh to sample the electronic Brillouin zone. The convergence parameters for structural relaxations include an energy difference within 10^{-6} eV and a Hellman-Feynman force within 10^{-4} eV/Å. For the calculation of surface states, we generate Wannier functions for

*bm418@cam.ac.uk

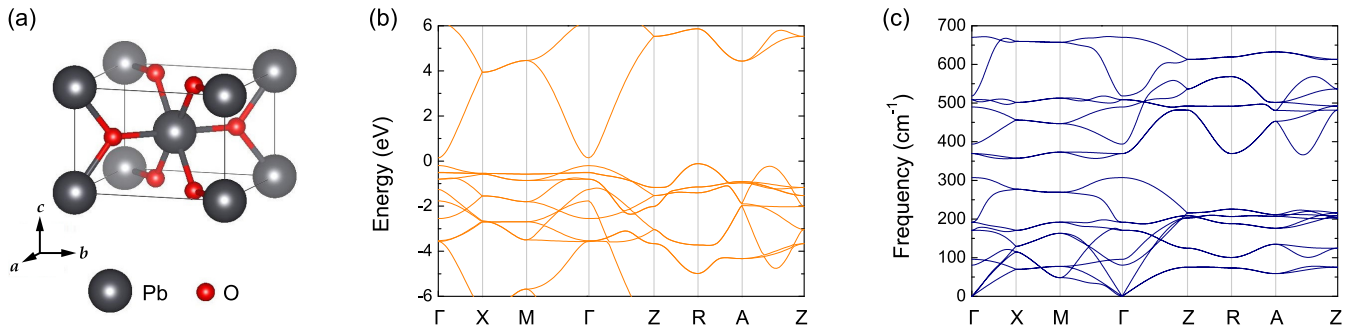


FIG. 1. (a) Unit cell of the crystal structure of β -PbO₂ with experimental lattice parameters $a = 4.961$ Å and $c = 3.385$ Å [22]. (b) Electronic band structure of β -PbO₂ calculated using the HSE06 functional. (c) Phonon dispersion of β -PbO₂ calculated using the HSE06 functional.

the s orbitals of lead and the p orbitals of oxygen using the WANNI90 package [28] combined with surface Green's functions as implemented in the WANNERTOOLS package [29,30]. The phonon dispersion, thermal expansion within the quasiharmonic approximation, and the electron-phonon interaction are calculated using the finite displacement method within the nondiagonal supercell approach [31,32], using coarse \mathbf{q} -point grids of size $4 \times 4 \times 4$ to sample the vibrational Brillouin zone. The temperature dependence of the band structures is calculated from vibrational averages along thermal lines [33,34].

Lead dioxide has been one of the most widely used functional oxides since the invention of the lead-acid battery in 1860 [35]. Figure 1(a) illustrates the most stable tetragonal β -PbO₂ phase (space group $P4_2/mnm$) in which each Pb atom is at the center of an O octahedral cage. We emphasize that our subsequent analysis of β -PbO₂ is based on first-principles DFT calculations using the HSE06 screened Coulomb hybrid density functional [24–26]. Compared to semilocal DFT, typically used for the study of β -PbO₂ [36,37], the HSE06 results show significantly better agreement with experimental measurements [38,39], providing a correct description of the structural, electronic, and vibrational properties of this material (a detailed validation study of the level of theory required to study β -PbO₂ can be found in the Supplemental Material [40]).

As shown in Fig. 1(b), PbO₂ is a semiconductor with the valence band maximum (VBM) at the R point and the

conduction band minimum (CBM) at the Γ point. The calculated indirect band gap of 0.24 eV and direct band gap of 0.34 eV at the Γ point agree well with previous calculations [39]. These results also agree well with hard x-ray photoelectron spectroscopy measurements, which indicate that β -PbO₂ is an intrinsic semiconductor, with the metallic behavior exhibited by some samples arising from a partially filled conduction band due to oxygen deficiency [35,41]. The HSE06 phonon dispersion in Fig. 1(c) shows no imaginary modes, thus indicating that the experimentally observed structure is stable at all temperatures. This is at odds with earlier DFT calculations using semilocal exchange-correlation functionals [37], but consistent with the fact that β -PbO₂ is the most stable phase under normal laboratory conditions [35]. Furthermore, the HSE06 Raman active modes are in better agreement with the experimental Raman spectrum [38] than the modes calculated using semilocal DFT (see Supplemental Material [40]).

The electronic structure of β -PbO₂ can be tuned from semiconducting to metallic by small variations of the lattice constants [39,42]. Interestingly, the normal band ordering at the Γ point is inverted under tensile lattice strain, resulting in nontrivial band topology [42]. To illustrate this, we carry out band-structure calculations under different tensile strains. Figure 2(a) presents the band gap at the Γ point as a function of strain in the (a, b) plane and strain along the c axis. The strain conditions for which the system has normal band ordering correspond to trivial insulators with the magnitude

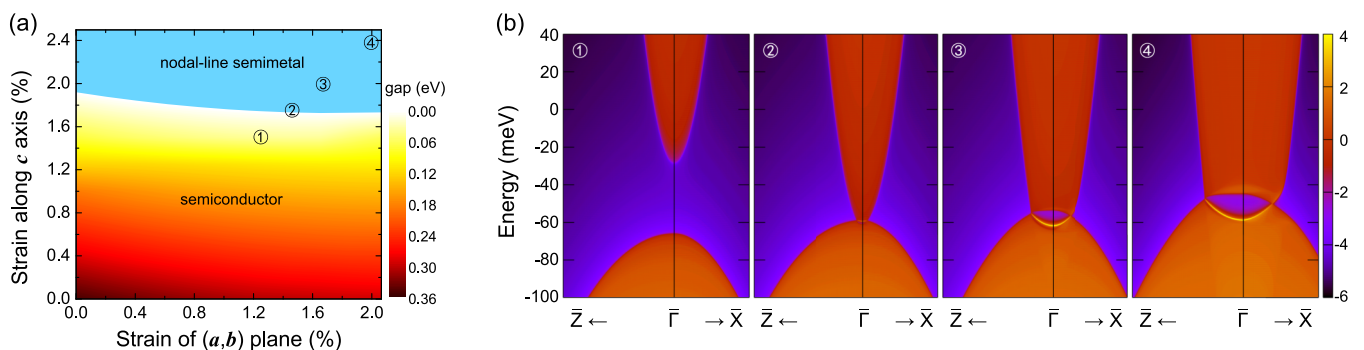


FIG. 2. (a) Calculated band gap at the Γ point of β -PbO₂ as a function of tensile strain. (b) Effect of tensile strain on the (010) surface states of β -PbO₂. A warmer color represents a higher surface contribution.

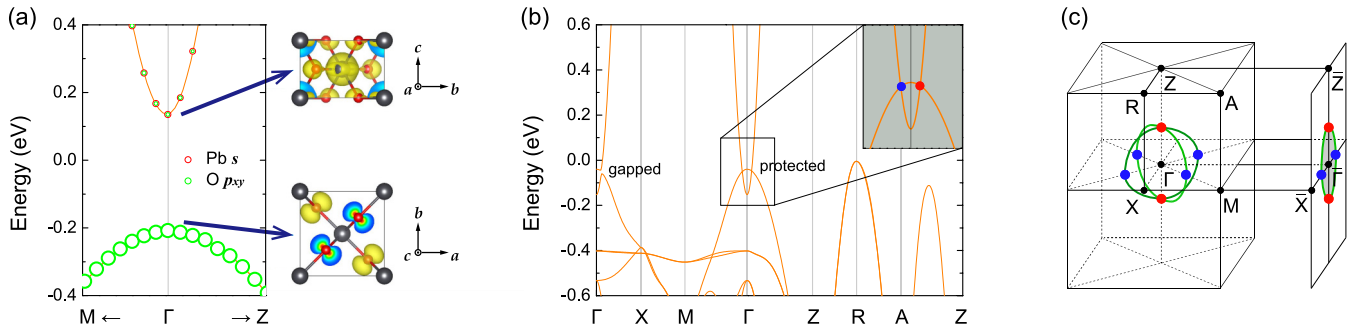


FIG. 3. Electronic structures for (a) unstrained and (b) strained $\beta\text{-PbO}_2$. Charge densities of the CBM and VBM states (isosurface = 0.008) are present in (a). (c) The bulk Brillouin zone and the surface Brillouin zone projected on the (010) surface are shown with two ring-shaped nodal lines on the $(1\bar{1}0)$ and (110) planes connecting the nodal points on the $M\text{-}\Gamma$ (blue dots) and $\Gamma\text{-}Z$ (red dots) high-symmetry lines.

of the band gap indicated by the red-yellow-white color scale, whereas those with inverted band ordering are marked by the cyan coloring. Increasing the c lattice constant closes the band gap, leading to a nodal-line semimetal phase (as we discuss below) at strains larger than around 1.9%. On the other hand, the band gap is insensitive to the strain in the (a, b) plane. Thus the c axis strain is a suitable tuning parameter to control the band topology of $\beta\text{-PbO}_2$.

To illustrate the strain effect and estimate its magnitude, we calculate the surface states under tensile strain in Fig. 2(b) on the basis of maximally localized Wannier functions [28] and surface Green's functions [29,30]. With an in-plane strain of 1.24% and an out-of-plane strain of 1.50%, the gap in the surface region decreases to 40 meV, and the conduction band moves below the Fermi energy due to the moving up of the VBM at the R point [panel 1 in Fig. 2(b)]. Under a modest strain of 1.45% and 1.75% in the (a, b) plane and along the c axis, a topological phase transition occurs as the conduction band moves slightly below the valence band at the Γ point [panel 2 in Fig. 2(b)]. Further increasing strain leads to the formation of distinct surface states around the Γ point [panels 3 and 4 in Fig. 2(b)]. A hallmark of nodal-line semimetals is the presence of two-dimensional drumheadlike surface states connecting the projected Dirac nodal points (the projection of the bulk nodal line onto the surface plane) [43,44]. These surface states with a divergent density of states can be detected by angle-resolved photoemission measurements [45], and may induce strong correlation phenomena such as high-temperature superconductivity [46].

To rationalize the behavior of the valence and conduction bands under tensile strain, we calculate the orbital characters near the Fermi energy. As shown in Fig. 3(a), the unstrained lattice has a normal band ordering at the Γ point with the VBM derived from the $2p_{xy}$ orbitals of oxygen, and the CBM predominantly consists of the $6s$ orbitals of lead that hybridize with the $2p_{xy}$ orbitals of oxygen. We also depict the real-space charge densities corresponding to the respective VBM and CBM at the Γ point in Fig. 3(a). The VBM at the Γ point is constituted of the O $2p_{xy}$ atomic orbitals which are oriented along the (a, b) plane of the primitive cell. This feature of the valence band can be seen as the establishment of a quasi-two-dimensional subsystem in the bulk. Instead, the CBM at the Γ point resembles the diffuse Pb $6s$ orbital which

has a three-dimensional character. This means that under uniaxial strain along the c direction the CBM experiences a reduced electron-electron repulsion arising from electrons of neighboring atoms (in the c direction) and as a consequence its energy decreases. In contrast, the aforementioned quasi-two-dimensional character of the valence band remains invariant under out-of-plane expansion. This leads to a relative shift of the VBM and the CBM that drives the observed band inversion. This explanation is consistent with the fact that under in-plane strain, no band inversion can be observed, which underpins the relevance of the out-of-plane anisotropy of the valence band. In this case, both valence and conduction band states experience similar stabilization effects upon expansion and therefore no crossing occurs. With larger tensile strains $\beta\text{-PbO}_2$ will revert to the standard behavior in which lattice expansion leads to the topologically trivial atomic limit.

To explain the formation of nodal lines, we examine the symmetry properties of $\beta\text{-PbO}_2$. For a fully relaxed unstrained crystal structure, $\beta\text{-PbO}_2$ is a trivial indirect band-gap semiconductor with the minimum direct band gap at the Γ point. Under tensile strain the band structure undergoes a band inversion at the Γ point. As shown in Fig. 3(b), under a modest strain of 2.07% in the (a, b) plane and 2.50% along the c axis [corresponding to panel 4 in Fig. 2(b)], the band gap at the Γ point is inverted with a band inversion energy of 0.11 eV, and two band crossing points are observed along the $M\text{-}\Gamma$ and $\Gamma\text{-}Z$ high-symmetry lines. The crossing points belong to two ring-shaped nodal lines on the $(1\bar{1}0)$ and (110) mirror symmetry planes, as shown in Fig. 3(c). In the absence of spin-orbit coupling, for each mirror plane the inverted band states have mirror eigenvalues -1 and $+1$, respectively, thus the two crossing bands cannot hybridize with each other and are therefore not gapped, forming a nodal line on the plane. The two nodal lines on the $(1\bar{1}0)$ and (110) planes are identical, which is similar to transition-metal rutile oxide PtO_2 [47]. For comparison, the band crossing on the $\Gamma\text{-}X$ high-symmetry line is not protected by mirror symmetry and therefore gapped.

We next evaluate the role of spin-orbit coupling in $\beta\text{-PbO}_2$. The crossing bands are comprised of the $6s$ states of the lead atoms and the $2p_{xy}$ states of the light oxygen atoms. As a consequence, none of these exhibit strong spin-orbit coupling effects, and the band structure and surface states with the inclusion of spin-orbit coupling are similar to those without

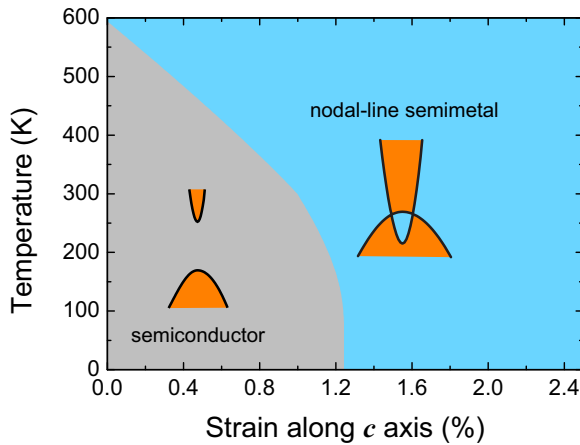


FIG. 4. Calculated strain-temperature phase diagram of β -PbO₂.

spin-orbit coupling. Technically, spin-orbit coupling breaks the SU(2) symmetry, generally gapping the nodal line with only one pair of Dirac points along the Γ -Z line remaining, as has been previously observed [36]. The Dirac points are protected by the fourfold screw rotation \tilde{C}_{4z} symmetry, which is a fourfold rotation about the z axis, followed by a translation by $(a/2, a/2, c/2)$ [47]. Thus the nodal-line semimetal evolves into a Dirac semimetal with the inclusion of spin-orbit coupling. Nonetheless, the weak spin-orbit coupling leads to a small gap of only 1.05 meV and the resulting physics resembles that of a nodal-line semimetal for temperatures over 12.2 K in which the bands merge due to the temperature-induced broadening (for further details on the spin-orbit coupling results, see the Supplemental Material [40]). The same physics holds for GW_0 band-structure calculations after taking exchange and correlation interactions of quasiparticles into consideration (for details on the GW_0 results, see the Supplemental Material [40]).

The behavior of β -PbO₂ under tensile strain discussed above indicates that, contrary to known topological materials, thermal expansion should promote topological order in β -PbO₂. In addition to thermal expansion, increasing temperature also enhances electron-phonon coupling. We find that electron-phonon coupling has a contribution similar to that of thermal expansion to the temperature-induced band inversion of β -PbO₂ (see Supplemental Material [40]). Figure 4 demonstrates the evolution of band topology as a function of temperature including both thermal expansion and electron-phonon coupling contributions, which promote the topological phase at high temperature. For unstrained PbO₂, the band gap closes above a temperature of 595 K, which is close to the temperature at which β -PbO₂ becomes unstable [35]. Above a strain of 1.26%, the system can be driven into a topological phase even at 0 K, and in the intermediate strain regime the temperature-promoted topological phase can be easily tuned to any intermediate temperature. We note that at 0 K the topological phase appears at a c strain of 1.26%, significantly lower than the required strain of around 1.9% at the static lattice level [see Fig. 2(a)]. This difference is a purely quantum effect arising from the zero-point motion of the lattice.

The unusual temperature-promoted topological order predicted in β -PbO₂ could be observed experimentally by exploiting the sensitivity of the transition temperature to the c -axis strain, which would enable the tuning of the transition temperature anywhere in the range 0–595 K. Both uniaxial tensile strain along the c axis, or three-dimensional tensile strain using a stool-like structure consisting of stylobate (substrate) and column (matrix) with appropriately matched lattice constants, could be used to scan over the phase diagram of β -PbO₂.

The relatively low melting temperature of β -PbO₂ [35] means that it is possible to grow highly crystalline films. The appropriate substrate and matrix materials can be chosen from candidates with lattice constants in the appropriate region of the diagram in Fig. 2(a). Using rutile TiO₂ as a substrate, with an in-plane lattice constant of $a = 4.594$ Å, would provide the in-plane compression of β -PbO₂ with an associated out-of-plane tension. Epitaxial growth of structurally analogous SnO₂ has been demonstrated on multiple orientations of a columbite CoNb₂O₆ substrate [48]. These substrates could be good starting points for exploring the topological phase diagram of β -PbO₂.

We also note that β -PbO₂ exhibits intrinsic defects that place the Fermi energy within the conduction bands [35,41]. This implies that the energy of the surface states will not coincide with the Fermi energy, and therefore the topological surface states will coexist with other nontopological surface states. Nonetheless, we remark that this is a common feature of many topological materials (see, e.g., Refs. [49,50]) that, although detrimental for the observation of isolated topological surface states, it facilitates the use of techniques such as angle-resolved photoemission spectroscopy for the detection of such states.

In summary, we have predicted that with a combination of thermal expansion and electron-phonon coupling, β -PbO₂ transforms from a trivial semiconductor at low temperatures to a topological semimetal at high temperatures. This behavior contrasts with that of known topological materials, most of which cannot hold topological order at high temperatures, with notorious examples including Chern insulators and topological superconductors which are currently restricted to a few degrees Kelvin at most. Our work proposes a microscopic picture of the chemical and physical mechanisms behind the interplay between topological order and temperature, and therefore provides a solid platform to search for topological materials whose topological order is robust at high temperatures. Such understanding paves the way for taking topological materials from the laboratory to technological devices.

I.B. and B.M. acknowledge support from the Winton Programme for the Physics of Sustainability. B.M. also acknowledges support from Robinson College, Cambridge, and the Cambridge Philosophical Society for a Henslow Research Fellowship. Part of the calculations was performed using resources provided by the Cambridge Tier-2 system operated by the University of Cambridge Research Computing Service [62] funded by EPSRC Tier-2 Capital Grant No. EP/P020259/1.

- [1] F. D. M. Haldane, Model for a Quantum Hall Effect without Landau Levels: Condensed-Matter Realization of the “Parity Anomaly”, *Phys. Rev. Lett.* **61**, 2015 (1988).
- [2] C.-Z. Chang, J. Zhang, X. Feng, J. Shen, Z. Zhang, M. Guo, K. Li, Y. Ou, P. Wei, L.-L. Wang, Z.-Q. Ji, Y. Feng, S. Ji, X. Chen, J. Jia, X. Dai, Z. Fang, S.-C. Zhang, K. He, Y. Wang, L. Lu, X.-C. Ma, and Q.-K. Xue, Experimental observation of the quantum anomalous Hall effect in a magnetic topological insulator, *Science* **340**, 167 (2013).
- [3] L. Fu and C. L. Kane, Superconducting Proximity Effect and Majorana Fermions at the Surface of a Topological Insulator, *Phys. Rev. Lett.* **100**, 096407 (2008).
- [4] X.-L. Qi, T. L. Hughes, S. Raghu, and S.-C. Zhang, Time-Reversal-Invariant Topological Superconductors and Superfluids in Two and Three Dimensions, *Phys. Rev. Lett.* **102**, 187001 (2009).
- [5] S. Nadj-Perge, I. K. Drozdov, J. Li, H. Chen, S. Jeon, J. Seo, A. H. MacDonald, B. A. Bernevig, and A. Yazdani, Observation of Majorana fermions in ferromagnetic atomic chains on a superconductor, *Science* **346**, 602 (2014).
- [6] B. Lian, X.-Q. Sun, A. Vaezi, X.-L. Qi, and S.-C. Zhang, Topological quantum computation based on chiral Majorana fermions, *Proc. Natl. Acad. Sci. USA* **115**, 10938 (2018).
- [7] M. Z. Hasan and C. L. Kane, Colloquium: Topological insulators, *Rev. Mod. Phys.* **82**, 3045 (2010).
- [8] X.-L. Qi and S.-C. Zhang, Topological insulators and superconductors, *Rev. Mod. Phys.* **83**, 1057 (2011).
- [9] P. Dziawa, B. J. Kowalski, K. Dybko, R. Buczko, A. Szczerbakow, M. Szot, E. Łusakowska, T. Balasubramanian, B. M. Wojek, M. H. Berntsen, O. Tjernberg, and T. Story, Topological crystalline insulator states in $\text{Pb}_{1-x}\text{Sn}_x\text{Se}$, *Nat. Mater.* **11**, 1023 (2012).
- [10] B. M. Wojek, M. H. Berntsen, V. Jonsson, A. Szczerbakow, P. Dziawa, B. J. Kowalski, T. Story, and O. Tjernberg, Direct observation and temperature control of the surface Dirac gap in a topological crystalline insulator, *Nat. Commun.* **6**, 8463 (2015).
- [11] B. Xu, L. X. Zhao, P. Marsik, E. Sheveleva, F. Lyzwa, Y. M. Dai, G. F. Chen, X. G. Qiu, and C. Bernhard, Temperature-Driven Topological Phase Transition and Intermediate Dirac Semimetal Phase in ZrTe_5 , *Phys. Rev. Lett.* **121**, 187401 (2018).
- [12] A. M. Kadykov, S. S. Krishtopenko, B. Jouault, W. Desrat, W. Knap, S. Ruffenach, C. Consejo, J. Torres, S. V. Morozov, N. N. Mikhailov, S. A. Dvoretiskii, and F. Teppe, Temperature-Induced Topological Phase Transition in HgTe Quantum Wells, *Phys. Rev. Lett.* **120**, 086401 (2018).
- [13] G. Krizman, B. A. Assaf, T. Phuphachong, G. Bauer, G. Springholz, L. A. de Vaulchier, and Y. Guldner, Dirac parameters and topological phase diagram of $\text{Pb}_{1-x}\text{Sn}_x\text{Se}$ from magnetospectroscopy, *Phys. Rev. B* **98**, 245202 (2018).
- [14] I. Garate, Phonon-Induced Topological Transitions and Crossovers in Dirac Materials, *Phys. Rev. Lett.* **110**, 046402 (2013).
- [15] K. Saha and I. Garate, Phonon-induced topological insulation, *Phys. Rev. B* **89**, 205103 (2014).
- [16] J. Kim and S.-H. Jhi, Topological phase transitions in group IV-VI semiconductors by phonons, *Phys. Rev. B* **92**, 125142 (2015).
- [17] B. Monserrat and D. Vanderbilt, Temperature Effects in the Band Structure of Topological Insulators, *Phys. Rev. Lett.* **117**, 226801 (2016).
- [18] G. Antonius and S. G. Louie, Temperature-Induced Topological Phase Transitions: Promoted versus Suppressed Nontrivial Topology, *Phys. Rev. Lett.* **117**, 246401 (2016).
- [19] L.-L. Wang, N. H. Jo, Y. Wu, Q. S. Wu, A. Kaminski, P. C. Canfield, and D. D. Johnson, Phonon-induced topological transition to a type-II Weyl semimetal, *Phys. Rev. B* **95**, 165114 (2017).
- [20] B. Monserrat and D. Vanderbilt, Temperature dependence of the bulk Rashba splitting in the bismuth tellurohalides, *Phys. Rev. Mater.* **1**, 054201 (2017).
- [21] M. M. Möller, G. A. Sawatzky, M. Franz, and M. Berciu, Type-II Dirac semimetal stabilized by electron-phonon coupling, *Nat. Commun.* **8**, 2267 (2017).
- [22] H. Harada, Y. Sasa, and M. Uda, Crystal data for $\beta\text{-PbO}_2$, *J. Appl. Crystallogr.* **14**, 141 (1981).
- [23] G. Kresse and J. Furthmüller, Efficient iterative schemes for *ab initio* total-energy calculations using a plane-wave basis set, *Phys. Rev. B* **54**, 11169 (1996).
- [24] J. Heyd, G. E. Scuseria, and M. Ernzerhof, Hybrid functionals based on a screened Coulomb potential, *J. Chem. Phys.* **118**, 8207 (2003).
- [25] J. Heyd, G. E. Scuseria, and M. Ernzerhof, Erratum: “Hybrid functionals based on a screened Coulomb potential” [J. Chem. Phys. **118**, 8207 (2003)], *J. Chem. Phys.* **124**, 219906 (2006).
- [26] J. E. Peralta, J. Heyd, G. E. Scuseria, and R. L. Martin, Spin-orbit splittings and energy band gaps calculated with the Heyd-Scuseria-Ernzerhof screened hybrid functional, *Phys. Rev. B* **74**, 073101 (2006).
- [27] J. P. Perdew, K. Burke, and M. Ernzerhof, Generalized Gradient Approximation Made Simple, *Phys. Rev. Lett.* **77**, 3865 (1996).
- [28] A. A. Mostofi, J. R. Yates, G. Pizzi, Y.-S. Lee, I. Souza, D. Vanderbilt, and N. Marzari, An updated version of WANNIERTOOLS: A tool for obtaining maximally-localised Wannier functions, *Comput. Phys. Commun.* **185**, 2309 (2014).
- [29] W. Zhang, R. Yu, H.-J. Zhang, X. Dai, and Z. Fang, First-principles studies of the three-dimensional strong topological insulators Bi_2Te_3 , Bi_2Se_3 and Sb_2Te_3 , *New J. Phys.* **12**, 065013 (2010).
- [30] Q. S. Wu, S. N. Zhang, H.-F. Song, M. Troyer, and A. A. Soluyanov, WANNIERTOOLS: An open-source software package for novel topological materials, *Comput. Phys. Commun.* **224**, 405 (2018).
- [31] J. H. Lloyd-Williams and B. Monserrat, Lattice dynamics and electron-phonon coupling calculations using nondiagonal supercells, *Phys. Rev. B* **92**, 184301 (2015).
- [32] B. Monserrat, Electron-phonon coupling from finite differences, *J. Phys.: Condens. Matter* **30**, 083001 (2018).
- [33] B. Monserrat, Vibrational averages along thermal lines, *Phys. Rev. B* **93**, 014302 (2016).
- [34] B. Monserrat, Correlation effects on electron-phonon coupling in semiconductors: Many-body theory along thermal lines, *Phys. Rev. B* **93**, 100301(R) (2016).
- [35] J. P. Carr and N. A. Hampson, Lead dioxide electrode, *Chem. Rev.* **72**, 679 (1972).
- [36] W. Wang, L. Deng, N. Jiao, P. Zhou, and L. Sun, Three-dimensional Dirac semimetal $\beta\text{-PbO}_2$, *Phys. Status Solidi RRL* **11**, 1700271 (2017).

- [37] T. Chen, D. Shao, P. Lu, X. Wang, J. Wu, J. Sun, and D. Xing, Anharmonic effect driven topological phase transition in PbO_2 predicted by first-principles calculations, *Phys. Rev. B* **98**, 144105 (2018).
- [38] L. Burgio, R. J. H. Clark, and S. Firth, Raman spectroscopy as a means for the identification of plattnerite (PbO_2), of lead pigments and of their degradation products, *Analyst* **126**, 222 (2001).
- [39] D. O. Scanlon, A. B. Kehoe, G. W. Watson, M. O. Jones, W. I. F. David, D. J. Payne, R. G. Egdell, P. P. Edwards, and A. Walsh, Nature of the Band Gap and Origin of the Conductivity of PbO_2 Revealed by Theory and Experiment, *Phys. Rev. Lett.* **107**, 246402 (2011).
- [40] See Supplemental Material at <http://link.aps.org/supplemental/10.1103/PhysRevB.100.161101> for the ground-state properties, band structure, and finite-temperature analysis of $\beta\text{-PbO}_2$, which includes Refs. [51–61].
- [41] D. J. Payne, G. Paolicelli, F. Offi, G. Panaccione, P. Lacovig, G. Beamson, A. Fondacaro, G. Monaco, G. Vanko, and R. G. Egdell, A study of core and valence levels in $\beta\text{-PbO}_2$ by hard X-ray photoemission, *J. Electron Spectrosc. Relat. Phenom.* **169**, 26 (2009).
- [42] F. Ma, Y. Jiao, G. Gao, Y. Gu, A. Bilic, S. Sanvito, and A. Du, Substantial band-gap tuning and a strain-controlled semiconductor to gapless/band-inverted semimetal transition in rutile lead/stannic dioxide, *ACS Appl. Mater. Interfaces* **8**, 25667 (2016).
- [43] A. A. Burkov, M. D. Hook, and L. Balents, Topological nodal semimetals, *Phys. Rev. B* **84**, 235126 (2011).
- [44] H. Weng, Y. Liang, Q. Xu, R. Yu, Z. Fang, X. Dai, and Y. Kawazoe, Topological node-line semimetal in three-dimensional graphene networks, *Phys. Rev. B* **92**, 045108 (2015).
- [45] G. Bian, T.-R. Chang, R. Sankar, S.-Y. Xu, H. Zheng, T. Neupert, C.-K. Chiu, S.-M. Huang, G. Chang, I. Belopolski, D. S. Sanchez, M. Neupane, N. Alidoust, C. Liu, BaoKai Wang, C.-C. Lee, H.-T. Jeng, Chenglong Zhang, Z. Yuan, S. Jia, A. Bansil, Fangcheng Chou, H. Lin, and M. Z. Hasan, Topological nodal-line fermions in spin-orbit metal PbTaSe_2 , *Nat. Commun.* **7**, 10556 (2016).
- [46] N. B. Kopnin, T. T. Heikkilä, and G. E. Volovik, High-temperature surface superconductivity in topological flat-band systems, *Phys. Rev. B* **83**, 220503(R) (2011).
- [47] R. Kim, B.-J. Yang, and C. H. Kim, Crystalline topological Dirac semimetal phase in rutile structure $\beta'\text{-PtO}_2$, *Phys. Rev. B* **99**, 045130 (2019).
- [48] J. Wittkamper, Z. Xu, B. Kombariah, F. Ram, M. De Graef, J. R. Kitchin, G. S. Rohrer, and P. A. Salvador, Competitive growth of scrutinyite ($\alpha\text{-PbO}_2$) and rutile polymorphs of SnO_2 on all orientations of columbite CoNb_2O_6 substrates, *Cryst. Growth Des.* **17**, 3929 (2017).
- [49] Y. L. Chen, J. G. Analytis, J.-H. Chu, Z. K. Liu, S.-K. Mo, X. L. Qi, H. J. Zhang, D. H. Lu, X. Dai, Z. Fang, S. C. Zhang, I. R. Fisher, Z. Hussain, and Z.-X. Shen, Experimental realization of a three-dimensional topological insulator, Bi_2Te_3 , *Science* **325**, 178 (2009).
- [50] R. Lou, P. Guo, M. Li, Q. Wang, Z. Liu, S. Sun, C. Li, X. Wu, Z. Wang, Z. Sun, D. Shen, Y. Huang, K. Liu, Z.-Y. Lu, H. Lei, H. Ding, and S. Wang, Experimental observation of bulk nodal lines and electronic surface states in ZrB_2 , *npj Quantum Mater.* **3**, 43 (2018).
- [51] Z. Wang and G. Wang, A new strongly topological node-line semimetal $\beta\text{-PbO}_2$, *Phys. Lett. A* **381**, 2856 (2017).
- [52] D. J. Payne, R. G. Egdell, D. S. L. Law, P.-A. Glans, T. Learmonth, K. E. Smith, J. Guo, A. Walsh, and G. W. Watson, Experimental and theoretical study of the electronic structures of $\alpha\text{-PbO}$ and $\alpha\text{-PbO}_2$, *J. Mater. Chem.* **17**, 267 (2007).
- [53] A. Marrazzo, M. Gibertini, D. Campi, N. Mounet, and N. Marzari, Prediction of a Large-Gap and Switchable Kane-Mele Quantum Spin Hall Insulator, *Phys. Rev. Lett.* **120**, 117701 (2018).
- [54] C. Fang, H. Weng, X. Dai, and Z. Fang, Topological nodal line semimetals, *Chin. Phys. B* **25**, 117106 (2016).
- [55] J. Liu and L. Balents, Correlation effects and quantum oscillations in topological nodal-loop semimetals, *Phys. Rev. B* **95**, 075426 (2017).
- [56] S. Pezzini, M. R. van Delft, L. M. Schoop, B. V. Lotsch, A. Carrington, M. I. Katsnelson, N. E. Hussey, and S. Wiedmann, Unconventional mass enhancement around the Dirac nodal loop in ZrSiS , *Nat. Phys.* **14**, 178 (2017).
- [57] M. Shishkin and G. Kresse, Implementation and performance of the frequency-dependent *GW* method within the PAW framework, *Phys. Rev. B* **74**, 035101 (2006).
- [58] M. Shishkin and G. Kresse, Self-consistent *GW* calculations for semiconductors and insulators, *Phys. Rev. B* **75**, 235102 (2007).
- [59] F. Fuchs, J. Furthmüller, F. Bechstedt, M. Shishkin, and G. Kresse, Quasiparticle band structure based on a generalized Kohn-Sham scheme, *Phys. Rev. B* **76**, 115109 (2007).
- [60] M. T. Dove, *Introduction to Lattice Dynamics* (Cambridge University Press, Cambridge, U.K., 1993).
- [61] B. Monserrat, G. J. Conduit, and R. J. Needs, Extracting semiconductor band gap zero-point corrections from experimental data, *Phys. Rev. B* **90**, 184302 (2014).
- [62] <http://www.hpc.cam.ac.uk>